

A Synthesis-Based Approach for Thermal-to-Visible Face Verification

Neehar Peri^{1,2}, Joshua Gleason^{1,2}, Carlos D. Castillo^{1,3}, Thirimachos Bourlai⁴, Vishal M. Patel^{1,3}, Rama Chellappa^{1,3}

¹ MUKH Technologies, ² University of Maryland, ³ Johns Hopkins University, ⁴ University of Georgia

Abstract—In recent years, visible-spectrum face verification systems have been shown to match expert forensic examiner recognition performance. However, such systems are ineffective in low-light and nighttime conditions. Thermal face imagery, which captures body heat emissions, effectively augments the visible spectrum, capturing discriminative facial features in scenes with limited illumination. Due to the increased cost and difficulty of obtaining diverse, paired thermal and visible spectrum datasets, algorithms and large-scale benchmarks for low-light recognition are limited. This paper presents an algorithm that achieves state-of-the-art performance on both the ARL-VTF and TUFTS multi-spectral face datasets. Importantly, we study the impact of face alignment, pixel-level correspondence, and identity classification with label smoothing for multi-spectral face synthesis and verification. We show that our proposed method is widely applicable, robust, and highly effective. In addition, we show that the proposed method significantly outperforms face frontalization methods on profile-to-frontal verification. Finally, we present MILAB-VTF(B), a challenging multi-spectral face dataset that is composed of paired thermal and visible videos. To the best of our knowledge, with face data from 400 subjects, this dataset represents the most extensive collection of publicly available indoor and long-range outdoor thermal-visible face imagery. Lastly, we show that our end-to-end thermal-to-visible face verification system provides strong performance on the MILAB-VTF(B) dataset.

I. INTRODUCTION

Face verification is concerned with the task of identifying if two face images correspond to the same identity (one-to-one matching). Web-scale visible-spectrum datasets and advances in training deep convolutional neural networks (DCNNs) have facilitated significant improvements in face verification, matching the recognition performance of forensic experts [24]. However, methods trained on visible-band face images often fail to generalize to low-light and nighttime conditions [2, 3]. Thermal imagery, particularly in the Long-Wave Infra-Red (LWIR, $7\mu\text{m} - 14\mu\text{m}$) and Mid-Wave Infra-Red (MWIR, $3\mu\text{m} - 5\mu\text{m}$) [25] bands, addresses limitations of the visible spectrum in low-light applications, effectively capturing discriminative information from body heat signatures. In order to leverage visible spectrum face verification pipelines in low-light scenes, recent works have proposed the task of thermal-to-visible spectrum face synthesis.

Standard Approach. The standard thermal-to-visible face synthesis pipeline consists of three stages: (1) detect and crop faces, (2) synthesize a corresponding visible-spectrum face for the thermal-spectrum input, and (3) extract discriminative features using a fixed feature extractor trained on visible-spectrum data. Significant distribution shifts between thermal and visible imagery make domain adaptation challenging.

In addition to identity labels, recent methods use additional annotations, including pose [33], part masks [19, 30], and attributes [7, 31, 32]. However, these methods may not effectively scale across diverse datasets and network architectures. The tasks of identity verification [23, 5] and re-identification [11, 18, 17] aim to learn a robust features embedding for identity matching. Since re-identification and multi-spectral face datasets typically have fewer identities than visible-band verification datasets, we also look to re-identification methods for inspiration.

Standard Datasets. Currently available thermal-visible datasets consist of face images captured under controlled conditions, in terms of background, illumination, standoff distance and pose. Unlike visible-spectrum face datasets, which often contain thousands of unique identities, with face images captured under constrained and unconstrained conditions, paired thermal-visible datasets are limited in terms of size and diversity in collection conditions. In order for dual-band (visible-thermal) verification pipelines to learn discriminative features, thermal and visible datasets must be composed of a sufficiently large number of identities.

Contributions. In this paper, we focus on advancing standard practices in thermal-to-visible face synthesis. We show that general-purpose domain adaptation algorithms can be highly effective, achieving state-of-the-art performance on both ARL-VTF [25] and TUFTS [21] datasets. In addition, we show that our method is surprisingly effective at frontal-to-profile matching, outperforming face frontalization methods [15, 33, 19, 30, 6]. Lastly, we introduce the largest to-date, long-range, unconstrained paired thermal-to-visible face dataset (MILAB-VTF(B)). The proposed method yields competitive performance on this dataset. We believe this novel dataset will be valuable in closing the data gap between visible-spectrum and multi-spectral datasets.

II. RELATED WORKS

In this section, we briefly discuss a limited subset of related work in developing robust end-to-end systems for thermal-to-visible face verification. In particular, we summarize prior face synthesis methods and highlight key features of large-scale publicly available datasets.

Domain Adaptation. Pix2Pix [16] introduces conditional adversarial networks that learn to adapt by generating realistic samples that match the target distribution. However, Pix2Pix requires paired examples. CycleGAN[34] introduces the cycle-consistency loss to learn a bi-directional mapping between two domains without paired examples. Several methods

have adapted the CycleGAN for task-specific applications. CyCADA [13] extends CycleGAN to enforce semantic consistency using an auxiliary task loss. Furthermore, BicycleGAN [35] addresses the problem of mapping two domains to sample diverse examples from a target distribution. More recently, contrastive unpaired translation (CUT) [22] uses contrastive learning to maintain the content of the input domain while learning the appearance of the target domain.

Face Synthesis. GAN-VFS [31] proposes an encoder-decoder structure that directly translates polarimetric images to the visible domain while enforcing a perceptual loss on intermediate features so that they closely resemble the intermediate feature embedding from a fine-tuned VGG-16 feature extractor. Similarly, [8] extends CycleGAN to enforce an ID loss to ensure features from synthesized images are close to the corresponding real image features and proposes a feature fusion of both polarimetric and visible image features to improve verification robustness. Unlike most synthesis based-methods, [9] directly adapts intermediate features from both thermal and visible images using truncated fixed feature extractors to learn a domain invariant representation for cross-domain matching. More recently, [7] introduced a method that incorporates facial attributes by pooling latent features with attribute features and synthesizes visible domain images at multiple scales to guide face synthesis effectively. Similarly, [20] considers multi-scale information for higher resolution generation with less training data using a series of cascade refinement networks.

Several methods focus on the sub-problem of face frontalization for profile-to-frontal matching. TP-GAN [15] proposes a dual-path generator that concatenates a coarsely generated frontal face with local profile facial features to generate a high-quality frontal view. [33] extends TP-GAN to jointly learn frontal face generation and discriminative feature embeddings for end-to-end face verification. [19, 30] use attention guided synthesis with part masks to frontalize profile face images. More recently, [6] proposes a contrastive learning approach for frontalization that achieves strong performance without additional part annotations.

We base our method on general-purpose domain adaptation algorithms tailored for the task of thermal-to-visible face synthesis.

Multi-Spectral Face Datasets. Several large-scale datasets exist for the task of thermal-to-visible face synthesis. The University of Notre Dame (UND) Dataset [4] contains 241 unique identities with four low-resolution images per identity. Next, the Natural Visible and Infrared Expression Database (NVIE) [29] shows subjects a video clip and captures subjects eliciting a wide range of facial expressions, with and without glasses. Data are synchronized manually after data collection. More recently, two volumes of the Multi-Modal Face Database (MMFD) [14] have been released, which provides synchronized imagery of visible, LWIR, and Polarimetric LWIR data at variable distances from the camera. ULFMT [10] contains unsynchronized MWIR and visible video recordings of 238 subjects capturing under variable conditions. The Tufts Face Database [21] is a multi-

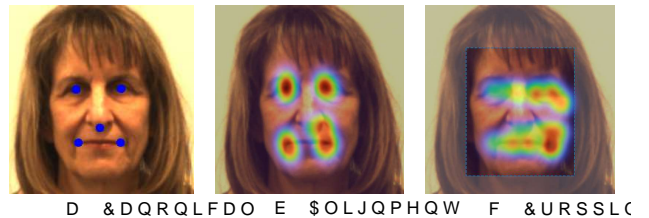


Fig. 1. We qualitatively demonstrate the impact of keypoint-based face alignment by plotting the distribution of ground truth keypoints (eyes, nose, mouth) after performing alignment and cropping, respectively, for profile-pose examples of an individual in the ARL-VTF dataset. Note that the cluster of keypoints after alignment (subfigure b) are closely correlated with the canonical keypoints for a front-pose face (subfigure a) while cropping (subfigure c) does not constrain keypoint locations. Tight clustering between samples due to alignment significantly improves both face synthesis and feature extraction.

modal dataset, capturing 100 subjects using LWIR, NIR, 2D, computer sketches, and 3D point clouds. In this paper, we are interested in the paired LWIR and visible images. Following the protocol established by prior work, we split the paired data in an 80-20 train-test split. The ARL-VTF dataset [25] is a recently introduced large-scale multi-spectral face dataset, containing time-synchronized paired LWIR and visible face with ground truth facial landmark annotations. This dataset contains 395 subjects under variable pose and expression.

III. ALIGN, TRANSLATE, AND CLASSIFY

Our proposed identity preserving thermal-to-visible face synthesis method is based on three key ideas: (1) keypoint-based face alignment, (2) pixel-level correspondence, and (3) feature-level identity classification. (1) is applied before training face synthesis, while (2) and (3) are constraints enforced during model training. We apply these three ideas to off-the-shelf domain adaptation methods, specifically Pix2Pix [16], CycleGAN [34], and CUT [22].

A. Keypoint-Based Face Alignment

Keypoint-based face alignment is a widely used technique to improve visible-spectrum face verification [26, 1, 5]. Alignment transforms the image such that key facial landmark locations (e.g., eyes, nose, mouth) are approximately constant in all images. Importantly, face alignment helps simplify face synthesis, particularly improving performance in synthesizing profile faces by reducing inter-sample variation, as shown in Figure 1. In addition, we find that synthesizing aligned faces further minimizes domain shift for feature extraction as visible-spectrum verification pipelines typically align faces before training. Surprisingly, we find that current thermal-to-visible face synthesis methods do not perform face alignment.

Face alignment consists of finding a similarity transform that maps a face onto standard locations of a fixed-size image. In face recognition, this is commonly done by determining the similarity transform that best maps a collection of estimated or annotated face keypoints to predefined positions, produced empirically by averaging over a subset of forward-facing samples with hand-labeled keypoints. In this work, we use ground-truth keypoints provided by the ARL-VTF dataset for training and inference and estimate keypoints using a detector,

as described in Section V-A, for the TUFTS and MILAB-VTF(B) datasets to perform face alignment. The similarity transform is solved using singular value decomposition as described in [28].

B. Pixel-Level Correspondence

Paired multi-spectral datasets are often calibrated to ensure pixel-wise correspondence between domains to facilitate supervised learning. Since we are interested in using off-the-shelf domain adaptation algorithms, many of which are unsupervised, we modify these methods to explicitly constrain the generated image to minimize the ℓ_1 distance with the ground truth visible image. Interestingly, we find that this additional regularization complements unsupervised image synthesis algorithms, as shown in Section VI-A.

C. Identity Classification with Label Smoothing

Reducing inter-identity distance in feature space has been shown to improve face verification from synthesized images. We extend the perceptual loss presented in [8] by enforcing an additional constraint such that all generated images of a particular class must cluster together. We illustrate the effect of this additional constraint in Figure 2. [11, 18] show that for datasets with a limited number of identities, as is the case in many paired thermal-to-visible datasets, label-smoothing in the cross-entropy loss effectively prevents over-fitting. We describe the identity loss function below:

$$\mathcal{L}_C = 1 - \cos(\Phi_F(\Phi_G(x_t)), \Phi_F(x_v)) + \sum_{i=1}^N -q_i \log p_i$$

$$q_i = \begin{cases} 1 - \frac{N-1}{N}\epsilon & i = y \\ \frac{\epsilon}{N} & o.w. \end{cases}$$

where Φ_F is a pretrained visible-spectrum face feature extractor, Φ_G is the thermal-to-visible synthesis network, x_t is the input thermal image, x_v is the ground truth visible image, ϵ is a noise constant, and N is the total number of classes. Using a fixed feature network to extract features from the synthesized image, we train a 3-layer MLP to learn a classifier to predict identity labels. In practice, the perceptual loss minimizes the cosine distance between normalized real and synthetic features. However, this constraint is ineffective if the features extracted from the ground truth image are not discriminative. The cross-entropy loss additionally ensures that all synthesized faces, particularly hard examples such as profile faces, are close in the embedding space.

D. Generic Formulation

We can generalize our proposed method as follows:

$$\mathcal{L} = \lambda_1 \cdot \mathcal{L}_G + \lambda_2 \cdot \mathcal{L}_1 + \lambda_3 \cdot \mathcal{L}_C$$

where λ_1 , λ_2 , & λ_3 are regularization constants, \mathcal{L}_G is the loss function of a general-purpose domain-adaptation algorithm, \mathcal{L}_1 is the pixel-wise loss between the synthesized and target images, and \mathcal{L}_C is the identity loss term described above. Our ablation study in Section VI-A suggests that each component is necessary independent of the synthesis network used.

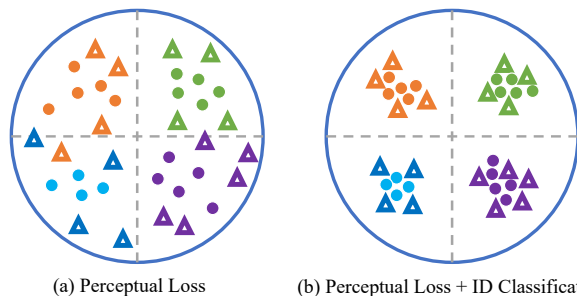


Fig. 2. The identity loss described in [8] attempts to minimize the ℓ_2 distance between the synthesized image features and real image features. This constraint assumes that features from synthetic faces of the same identity are close together in feature space. Although this is valid for easy examples (shown as circles), it may not hold for hard examples (shown as triangles).

IV. MILAB-VTF(B): A LARGE-SCALE DATASET FOR UNCONSTRAINED THERMAL-TO-VISIBLE SYNTHESIS

In this section, we present MILAB-VTF(B), a challenging large-scale multi-spectral face dataset collected on the campus of the University of Georgia. This dataset captures unsynchronized paired thermal and visible data from 400 identities in varied poses and distances. Sample images from this dataset are shown in Figure 3. We compare MILAB-VTF(B) to other multi-modal datasets in Figure 4.

Dataset Collection. The data was collected over five weeks, starting in February 2021. The dataset contains 400 subjects, each of whom completed an Institutional Review Board (IRB) approved consent form before image acquisition. The dataset has unsynchronized paired thermal and visible videos indoors at 1.5 meters and outdoors at 100, 200, 300, and 400 meters. Each subject was recorded for approximately 30 seconds. Participants were instructed to articulate their heads $\pm 60^\circ$ left-and-right and up-and-down in each scene. Indoor scenes were captured using a Canon Mark IV (Visible) and a FLIR A8581 (MWIR). Outdoor scenes were captured by a Nikon P1000 (Visible) and a FLIR RS8513 (MWIR).

Training and Evaluation Protocol. The MILAB-VTF(B) dataset provides unsynchronized, paired thermal-visible

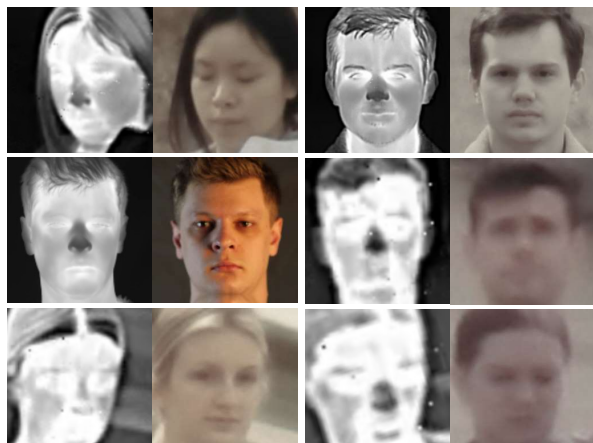
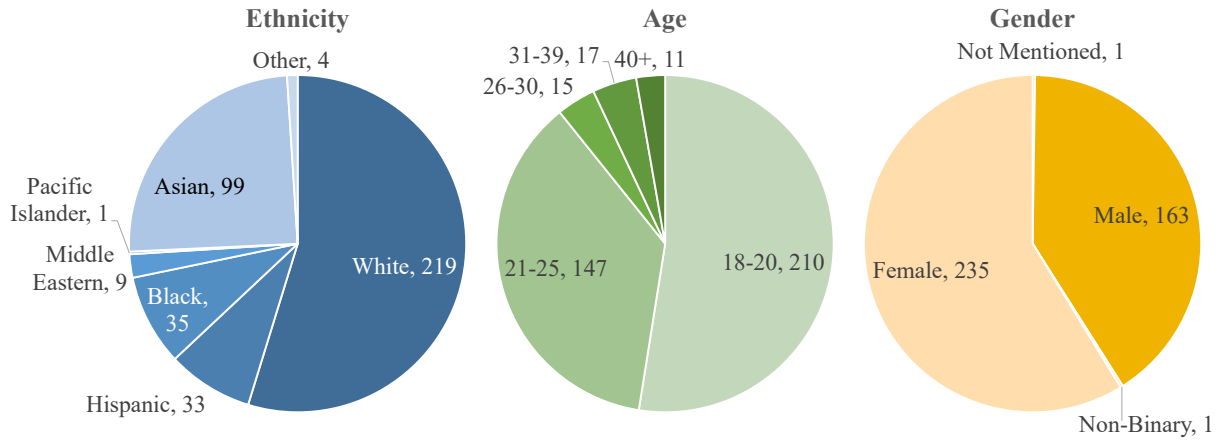


Fig. 3. We present representative examples of paired thermal-visible data from the MILAB-VTF(B) dataset. Importantly, this dataset contains diverse lighting and image quality due to the large range of collection distances not found in other multi-spectral datasets.



Dataset	Modalities	Subjects	Variability	IR Resolution (W × H)	Range (m)
UND [4]	LWIR, Visible	241	I, E, T	320 × 240	Unspecified
NVIE [29]	LWIR, Mono	215	I, E, G	320 × 240	0.75
ULFMT [10]	MWIR, Visible	238	P, E, T, G	640 × 512	1.0
ARL-MMFD [14]	P-L, LWIR, Visible	111	E	640 × 480 (LW)	2.5, 5.0, 7.5
Tufts [21]	NWIR, LWIR, Visible	100	P, E	336 × 256	1.5
ARL-VTF [25]	LWIR, Visible, Mono	395	P, E, G	630 × 512	2.1
MILAB-VTF(B) (Ours)	MWIR, Visible	400	P, L, I _N , E _N , O _N	1280 × 1024	1.5, 100, 200, 300, 400

Fig. 4. We denote the variable characteristics of each dataset as follows: (P)ose, (I)llumination, (E)xpression, (T)ime-lapse, (G)lasses, (O)clusion, and (L)ocation. We use the subscript N to identify characteristics that occur due to natural outdoor conditions (i.e. sunlight, clouds, and wind). MILAB-VTF(B) uniquely captures high-resolution paired thermal and visible scenes outdoors at long ranges. Importantly, the dataset is diverse with respect to ethnicity, age, and gender. This table is adapted from [25].

frames and anonymized identifiers for each subject. We provide algorithmically generated frame synchronization between thermal and visible videos, face bounding boxes, and keypoints, but encourage researchers to develop end-to-end multi-spectral face verification pipelines.

We select 320 identities for training and sequester 80 identities for evaluation. Following standard face verification protocols, we create gallery and query sets from the sequestered data. Specifically, we create four non-overlapping galleries and four non-overlapping query sets by splitting the evaluation data by pose (i.e., frontal/profile) and location (i.e. indoor/outdoor).

V. END-TO-END THERMAL-TO-VISIBLE SYNTHESIS

In this section, we briefly describe our end-to-end thermal-to-visible face verification pipeline. First, we present the face detection and keypoint regression models required to pre-process data before thermal-to-visible synthesis. Next, we highlight our automatic temporal alignment algorithm for synchronizing the visible and thermal data streams in the MILAB-VTF(B) dataset. We leverage this end-to-end pipeline to train and evaluate both the TUFTS [21] and MILAB-VTF(B) datasets.

A. Face Detection and Keypoint Regression

Face localization and keypoint regression are essential pre-processing steps in end-to-end thermal-to-visible face verification. Importantly, we find that we can jointly train a

single model to address both the thermal and visible domains, improving label efficiency. Given the limited availability of face bounding boxes and keypoint detections in the thermal domain, we can use models trained on visible images to bootstrap multi-spectral domain training. Using a large set of publicly available face bounding boxes for visible images and a small set of face bounding boxes for thermal images, we train a Faster-RCNN [27] detector to localize faces. We propose a novel multi-task architecture for facial landmark localization. Our keypoint regressor outputs four sets of keypoints at different locations using a truncated ResNet-50 [12] backbone, followed by four different encoder-decoder heads, representing different densities of keypoints, respectively. The encoder-decoder heads learn a low-dimensional representation of the keypoint layout for each family of keypoints. From the penultimate (2048-dimensional) layer of the ResNet backbone, we predict the four families of keypoints, as well as yaw-roll-pitch. We have implemented an inference engine that uses multiple crops of the detected face and applies a fast implementation of a RANSAC-based method to aggregate the locations of the keypoints at inference time. Given keypoint annotations, we can infer face bounding box locations to iteratively train our visible and thermal face detector.

B. Pairwise Image Synchronization

Since the MILAB-VTF(B) dataset does not provide temporally aligned paired videos, we propose a simple synchro-

nization algorithm using keypoint-based face alignment. We refer readers to [28] for the alignment optimization.

For each frame in paired thermal and visible videos, we extract facial keypoints. We align the keypoints into the aligned domain using a similarity transform obtained using least-squares optimization. Transforming both thermal and visible keypoints into the aligned domain implies that keypoints from corresponding visible and thermal images should match. Using this insight, we perform a greedy matching between thermal and visible frames to minimize the normalized ℓ_2 distance between the transformed visible and thermal keypoints. This alignment provides us corresponding approximate thermal/visible pairs, allowing us to leverage supervised algorithms for thermal-to-visible face synthesis.

This approach allows for many-to-one matching, whereby multiple visible frames can be mapped to the same thermal frame. Moreover, this algorithm does not preserve the temporal characteristics of the input video. Since we only consider keypoints, facial expression, hair, and ocular movement between synchronized thermal and visible frames may not be consistent. However, we find that this simple approach works well in practice.

VI. EXPERIMENTS AND RESULTS

In this section, we highlight the performance of our proposed method on the ARL-VTF and TUFTS datasets and establish a strong baseline for the MILAB-VTF(B) dataset. In addition, we conduct ablation studies on the ARL-VTF dataset using three off-the-shelf domain adaptation methods [16, 34, 22]. Following standard face verification evaluation protocols, we report verification performance using the area under the curve (AUC), equal error rate (EER), and true accept rate (TAR) at false accept rates (FAR) of 1% and 5%.

Implementation Details. We train each thermal-to-visible face synthesis model for twenty-five epochs and use the Adam optimizer with a learning rate of $2e-3$. Importantly, we find that batch size has a significant impact on face verification performance. Smaller batch sizes work best, and we opt to train our models with a batch size of 4. Moreover, we find that training for a large number of epochs causes significant overfitting. We synthesize 128×128 thumbnails and resize the output image using nearest-neighbor interpolation to match the input size requirement of the fixed feature extractor. We perform double-flip augmentations and average the extracted features before computing verification metrics. We report average performance across all gallery and query splits in the main paper and refer the reader to the supplemental material for detailed cohort analysis.

A. Ablation Study Using the ARL-VTF Dataset

We use Pix2Pix [16], CycleGAN [34], and CUT [22] as backbone architectures to demonstrate the broad applicability of our proposed methods, as shown in Table I. Our baseline models emulate current practices, simply cropping thermal faces, synthesizing visible faces, and extracting features with VGGFace [23]. The batch size, learning rate, and number of training epochs remain constant through the ablation study.

Each row in Table I builds upon the previous results, which are each described in the following sections.

Impact of Face Alignment. Many standard thermal-to-visible face synthesis algorithms tightly crop a subject’s face to isolate facial features for synthesis. However, we find that aligning the keypoints to canonical locations before synthesis is an important pre-processing step that considerably impacts feature extraction quality and face verification performance. We find that alignment improves performance across all models. Importantly, we highlight that alignment produces significant improvements in unsupervised models. AUC increases by more than 40% for both CycleGAN and CUT. Surprisingly, we find that CycleGAN and CUT, both unsupervised domain adaptation algorithms perform better than Pix2Pix, indicating that further study into unsupervised algorithms may be warranted. We posit that unsupervised synthesis is easier after performing alignment because key facial features are always in approximately the same location, allowing an unsupervised model to learn better features.

Impact of Pixel-wise Correspondence. Given that many thermal-to-visible synthesis datasets provide corresponding images in both domains, it is natural to extend unsupervised algorithms by enforcing an additional constraint such that the synthesized image minimizes the ℓ_1 distance with the ground truth visible image. We extend both CycleGAN and CUT such that the generated images minimize the pixel-wise distance from the ground truth and observe a modest performance improvement. This improvement indicates that the supervisory signal from the ℓ_1 pixel-wise loss is complementary to the unsupervised losses in both CycleGAN and CUT, respectively. Note that since Pix2Pix already enforces this constraint, we omit this row.

Impact of Identity Loss. Both prior modifications improve the visual quality of generated images but do not explicitly constrain the resulting feature embedding. Here, we minimize the cosine distance between the features from the generated visible image and the real visible image, this groups the

TABLE I
ABLATION STUDY USING THE ARL-VTF DATASET

Model	AUC \uparrow	EER \downarrow	TAR@1% \uparrow	TAR@5% \uparrow
Pix2Pix [16]	85.3	22.4	21.6	43.6
+ Alignment	90.1	17.8	30.9	58.3
+ \mathcal{L}_1 Pixel Loss	-	-	-	-
+ Identity Loss	91.3	16	33.6	62.6
w/ ArcFace	83.8	24.4	23	44.8
Cycle-GAN [34]	51.1	49	1.8	5.7
+ Alignment	92.1	14	54.7	71.9
+ \mathcal{L}_1 Pixel Loss	94	11.7	58.1	79.3
+ Identity Loss	95.3	10.7	58.8	81.1
w/ ArcFace	96.8	9.2	68.7	85.2
CUT [22]	52.6	47.9	1.4	5.7
+ Alignment	93.5	13.6	52.7	74.6
+ \mathcal{L}_1 Pixel Loss	95.4	10.3	61.5	80.4
+ Identity Loss	95.9	9.9	64.3	82.6
w/ ArcFace	97.7	6.9	77.2	90.5

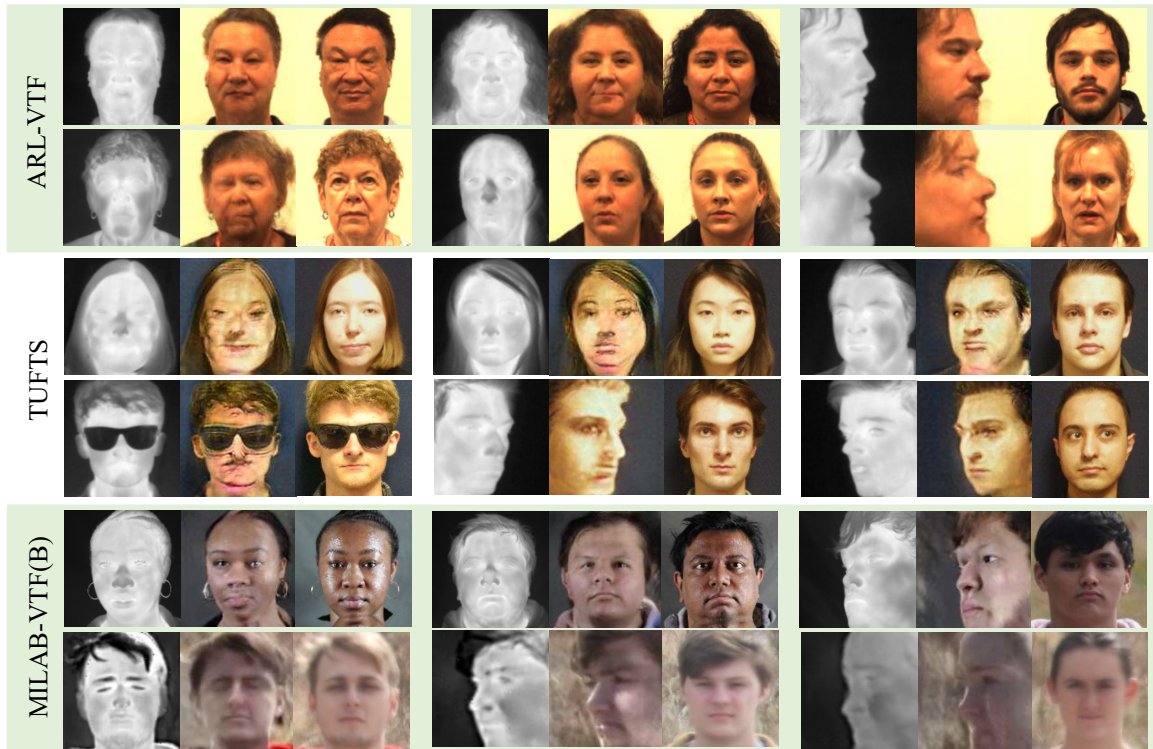


Fig. 5. We share synthesized images using CUT-ATC from the ARL-VTF, TUFTS, and MILAB-VTF(B) datasets. Each 3-tuple of images contains the thermal spectrum input, the synthesized output, and a frontal-pose visible image from the same identity. The limited data of the TUFTS dataset and atmospheric turbulence in the MILAB-VTF(B) dataset significantly degrade perceptual quality. Textures, particularly in hair, are not well preserved.

features of the generated image close to the features of the real images. In addition, we also use cross-entropy loss with label smoothing to classify the features from the generated image into one of the N classes in the training set. This additional loss minimizes the inter-class distance despite variations in pose and expression. We set $\epsilon=0.1$ and $N=236$ for this study. Importantly, we note that label smoothing is an effective way to prevent overfitting on the training set, facilitating greater generalization [11, 18]. Table I highlights that this feature classification provides small but consistent improvement across all tested models.

Impact of Feature Extractor. Many state-of-the-art algorithms use VGGFace [23] to extract discriminative features from the penultimate fully-connected layer. To facilitate a fair comparison with other methods, we perform all ablation studies using this feature extractor unless explicitly noted. We highlight that the improved performance of our baseline is not just a result of using a more robust feature extractor, but rather due to effective domain adaptation. Surprisingly, we find that ArcFace [5], a feature extractor that improves considerably upon VGGFace on visible domain benchmarks, performs worse when extracting features from images synthesized using Pix2Pix. This suggests that the effectiveness of the feature extractor is dependent on the network architecture. We posit that ArcFace is more sensitive to domain shift caused by synthetic imagery, indicating that CycleGAN and CUT more closely approximate the distribution of real faces.

B. State-of-the-Art Comparison

We compare the proposed method against general-purpose methods and task-specific methods that focus on frontal-to-profile matching. We find that our proposed method significantly improves upon the state-of-the-art. As shown in Table I, CUT, augmented by our proposed modifications, performs best. We compare this model, denoted as CUT-ATC, with other leading methods on the ARL-VTF and TUFTS face datasets.

TABLE II
ARL-VTF STATE-OF-THE-ART COMPARISON

Model	AUC \uparrow	EER \downarrow	TAR@1% \uparrow	TAR@5% \uparrow
GANVFS [31]	85.7	20.0	42.5	57.9
Multi-AP-GAN [7]	87.0	18.1	49.1	63.4
Fondje et. al. [9]	90.1	13.1	73.0	78.8
CUT-ATC	97.7	6.9	77.2	90.5

Our proposed model improves upon recent methods for thermal-to-visible synthesis. Table II demonstrates that we improve on all metrics, specifically increasing AUC by 7.6%, reducing EER by 6.2%, and improving TAR at FAR=1% and FAR=5% by 4.2% and 11.7%, respectively. Fondje et. al. [9] perform better than prior methods because they align their input images similar to our proposed approach. However, rather than trying to learn domain agnostic features from a small dataset, we extract features from synthesized faces using ArcFace [5].

TABLE III
TUFTS STATE-OF-THE-ART COMPARISON

Model	AUC \uparrow	EER \downarrow	TAR@1% \uparrow	TAR@5% \uparrow
GANVFS [31]	73.8	32.3	-	-
CRN + CL [20]	74.9	31.7	-	-
Multi-AP-GAN [7]	77.4	29.9	-	-
CUT-ATC	87.4	21.3	26.2	50.6

The TUFTS face dataset is challenging due to the limited number of training examples. Despite this limitation, Table III shows that our proposed method similarly improves on all reported metrics. Specifically, we improve AUC by 10.0% and reduce EER by 8.5%. With only 1200 paired visible-thermal training images, over-fitting is a significant concern.

TABLE IV
ARL-VTF COMPARISON WITH FACE FRONTALIZATION METHODS
GALLERY 0010

Query 00 Pose	AUC \uparrow	EER \downarrow	TAR@1% \uparrow	TAR@5% \uparrow
PIM [33]	68.7	36.6	5.4	16.5
M2FPA [19]	75.0	32.3	5.7	20.3
DA-GAN [30]	75.6	31.2	6.9	22.2
DAL-GAN [6]	77.5	29.1	8.2	25.9
CUT-ATC	94.1	12.1	63.0	80.9
Query 10 Pose	AUC \uparrow	EER \downarrow	TAR@1% \uparrow	TAR@5% \uparrow
PIM [33]	73.3	32.7	6.0	20.4
M2FPA [19]	77.0	29.8	9.5	23.4
DA-GAN [30]	75.8	30.7	8.4	23.6
DAL-GAN [6]	82.2	25.1	10.8	30.6
CUT-ATC	95.6	11.0	67.9	82.7

Frontal-to-profile matching is a difficult sub-problem within face verification because there is little spatial overlap between both poses. Moreover, thermal-to-visible synthesis adds additional complexity, requiring matching between synthesized and real faces. Face frontalization methods explicitly attempt to address this sub-problem by synthesizing frontal faces given a profile view for better spatial overlap when matching identities. In general, these task-specific methods are usually more effective at frontal-to-profile matching than general-purpose thermal-to-visible face synthesis approaches. However, our proposed modifications, particularly aligning profile faces to canonical coordinates, improves matching performance, as demonstrated in Table IV. In particular, we improve AUC by approximately 15%, reduce EER by 15%, and improve TAR at both FAR=1% and FAR=5% by approximately 50% on the ARL-VTF dataset. Applying our general-purpose modifications to existing face frontalization methods may result in even better profile-to-frontal matching performance and warrants further investigation.

Similarly, we find that our proposed method improves over face frontalization methods on the TUFTS dataset. As shown in Table V we improve AUC by 8.9%, reduce EER by 7.3%, and improve TAR at FAR=1% and FAR=5% by 13.5% and 24.6%, respectively. We highlight that our proposed approach remains effective despite the small size of the TUFTS dataset.

TABLE V
TUFTS COMPARISON WITH FACE FRONTALIZATION METHODS
GALLERY FRONTAL

Query Profile	AUC \uparrow	EER \downarrow	TAR@1% \uparrow	TAR@5% \uparrow
PIM [33]	72.8	34.1	8.8	21.0
M2FPA [19]	75.1	31.2	8.3	23.4
DA-GAN [30]	75.2	31.1	10.4	26.2
DAL-GAN [6]	78.7	28.4	10.4	27.1
CUT-ATC	87.6	21.1	23.9	51.7

C. Baseline on MILAB-VTF(B)

We train our proposed models on the MILAB-VTF(B) dataset and report the average performance on each of the evaluation protocols. We denote the best-performing model and feature extractor combination from Table I for each backbone architecture with the ATC identifier.

TABLE VI
MILAB-VTF(B) DATASET BASELINE PERFORMANCE

Model	AUC \uparrow	EER \downarrow	TAR@1% \uparrow	TAR@5% \uparrow
Pix2Pix-ATC	59.3	43.4	2.7	10.5
CycleGAN-ATC	54.9	46.4	1.5	7.1
CUT-ATC	68.8	36.3	8.0	22.3

Based on the evaluation results in Table VI, MILAB-VTF(B) is more challenging than prior datasets. Our method, which achieves the state-of-the-art for ARL-VTF and TUFTS, performs significantly worse on MILAB-VTF(B). This is likely due to atmospheric turbulence and other visual artifacts resulting from long-distance data capture. Moreover, perfect pixel-wise correspondence is not guaranteed in MILAB-VTF(B) because we use an imperfect keypoint detector. This issue is further exacerbated for tiny faces, where a few pixels of error can cause significant misalignment. We did not specifically design our method to address the unique challenges presented by MILAB-VTF(B). However, we look forward to future investigations.

VII. CONCLUSION

In this paper, we present an algorithm and a new challenging dataset for thermal-to-visible face verification. Through extensive experimentation, we show that appropriate modifications to off-the-shelf domain adaptation algorithms are widely applicable and significantly improve upon the state-of-the-art. Importantly, our experimental results suggest that face alignment, rather than cropping, is a simple modification that should be embraced in future visible-to-thermal synthesis and verification works. Despite the effectiveness of our baseline, MILAB-VTF(B) remains a challenging dataset that merits further exploration.

VIII. ACKNOWLEDGEMENTS

This work was partially supported by an STTR Phase II contract W911QX20C0022 from the US Army Research Laboratory, Adelphi, MD.

REFERENCES

- [1] A. Bansal, C. D. Castillo, R. Ranjan, and R. Chellappa. “The Do’s and Don’ts for CNN-Based Face Verification”. In: *ICCV Workshops*. IEEE Computer Society, 2017, pp. 2545–2554.
- [2] T. Bourlai. *Face Recognition Across the Imaging Spectrum*. Springer, 2016.
- [3] T. Bourlai and L. Hornak. “Face Recognition Outside the Visible Spectrum”. In: *Image and Vision Computing* (2016).
- [4] X. Chen, P. J. Flynn, and K. W. Bowyer. “Visible Light and Infrared Face Recognition”. In: *ACM Workshop on Multimodal User Authentication*. ACM, 2003, pp. 48–55.
- [5] J. Deng, J. Guo, N. Xue, and S. Zafeiriou. “ArcFace: Additive Angular Margin Loss for Deep Face Recognition”. In: *CVPR*. 2019, pp. 4690–4699.
- [6] X. Di, S. Hu, and VM. Patel. “Heterogeneous Face Frontalization via Domain Agnostic Learning”. In: *IEEE Conference on Face and Gesture* (2021).
- [7] X. Di, BS. Riggan, S. Hu, NJ. Short, and VM. Patel. “Multi-Scale Thermal to Visible Face Verification via Attribute Guided Synthesis”. In: *IEEE Trans. Biom. Behav. Identity Sci.* 3.2 (2021), pp. 266–280.
- [8] X. Di, BS. Riggan, S. Hu, NJ. Short, and VM. Patel. “Polarimetric Thermal to Visible Face Verification via Self-Attention Guided Synthesis”. In: *International Conference on Biometrics, ICB*. IEEE, 2019.
- [9] CN. Fondje, S. Hu, NJ. Short, and BS. Riggan. “Cross-Domain Identification for Thermal-to-Visible Face Recognition”. In: *IEEE International Joint Conference on Biometrics, IJCB*. IEEE, 2020, pp. 1–9.
- [10] RS. Ghiass, H. Bendar, and X. Maldague. “Universite Laval Face Motion and Time-Lapse Video Database (UL-FMTV)”. In: *Technical Report* (2018).
- [11] H., Y. Gu, X. Liao, S. Lai, and W. Jiang. “Bag of Tricks and a Strong Baseline for Deep Person Re-Identification”. In: *IEEE CVPR Workshops*. 2019, pp. 1487–1495.
- [12] K. He, X. Zhang, S. Ren, and J. Sun. “Deep Residual Learning for Image Recognition”. In: *CVPR*. IEEE Computer Society, 2016, pp. 770–778.
- [13] J. Hoffman, E. Tzeng, T. Park, JY. Zhu, P. Isola, K. Saenko, AA. Efros, and T. Darrell. “CyCADA: Cycle-Consistent Adversarial Domain Adaptation”. In: *ICML*. Proceedings of Machine Learning Research. PMLR, 2018.
- [14] S. Hu, N. J. Short, B. S. Riggan, C. Gordon, K. P. Gurton, M. Thielke, P. Gurram, and A. L. Chan. “A Polarimetric Thermal Database for Face Recognition Research”. In: *IEEE CVPR Workshop*. IEEE Computer Society, 2016, pp. 187–194.
- [15] R. Huang, S. Zhang, T. Li, and Ran He. “Beyond Face Rotation: Global and Local Perception GAN for Photorealistic and Identity Preserving Frontal View Synthesis”. In: *IEEE International Conference on Computer Vision, ICCV*. IEEE Computer Society, 2017, pp. 2458–2467.
- [16] P. Isola, JY. Zhu, T. Zhou, and AA. Efros. “Image-to-Image Translation with Conditional Adversarial Networks”. In: *CVPR*. IEEE Computer Society, 2017, pp. 5967–5976.
- [17] P. Khorramshahi, A. Kumar, N. Peri, SS. Rambhatla, JC. Chen, and R. Chellappa. “A Dual-Path Model With Adaptive Attention for Vehicle Re-Identification”. In: *IEEE/CVF ICCV*. IEEE, 2019, pp. 6131–6140.
- [18] P. Khorramshahi, N. Peri, JC. Chen, and Rama Chellappa. “The Devil Is in the Details: Self-supervised Attention for Vehicle Re-identification”. In: *ECCV*. Vol. 12359. Lecture Notes in Computer Science. Springer, 2020, pp. 369–386.
- [19] P. Li, X. Wu, Y. Hu, R. He, and Z. Sun. “M2FPA: A Multi-Yaw Multi-Pitch High-Quality Database and Benchmark for Facial Pose Analysis”. In: *ICCV* (2019).
- [20] K. Mallat, N. Damer, F. Boutros, A. Kuijper, and JL. Dugelay. “Cross-spectrum Thermal to Visible Face Recognition Based on Cascaded Image Synthesis”. In: *International Conference on Biometrics, ICB*. IEEE, 2019.
- [21] K. Panetta, A. Samani, X. Yuan, Q. Wan, SS. Agaian, S. Rajeev, S. Kamath K. M, R. Rajendran, S. Paramathma Rao, A. Kaszowska, and HA. Taylor. “A Comprehensive Database for Benchmarking Imaging Systems”. In: *IEEE Trans. Pattern Anal. Mach. Intell.* (2020), pp. 509–520.
- [22] T. Park, AA. Efros, R. Zhang, and JY. Zhu. “Contrastive Learning for Unpaired Image-to-Image Translation”. In: *ECCV*. Vol. 12354. Lecture Notes in Computer Science. Springer, 2020, pp. 319–345.
- [23] O. M. Parkhi, A. Vedaldi, and A. Zisserman. “Deep Face Recognition”. In: *BMVC*. BMVA Press, 2015, pp. 41.1–41.12.
- [24] P. J. Phillips, A. N. Yates, Y. Hu, C. A. Hahn, E. Noyes, K. Jackson, J. G. Cavazos, G. Jeckeln, R. Ranjan, S. Sankaranarayanan, J. Chen, C. D. Castillo, R. Chellappa, D. White, and A. J. O’Toole. “Face Recognition Accuracy of Forensic Examiners, Superrecognizers, and Face Recognition Algorithms”. In: *Proceedings of the National Academy of Sciences* 115.24 (2018), pp. 6171–6176. ISSN: 0027-8424.
- [25] D. Poster, M. Thielke, R. Nguyen, S. Rajaraman, X. Di, C. N. Fondje, V. M. Patel, N. J. Short, B. S. Riggan, N. M. Nasrabadi, and S. Hu. “A Large-Scale, Time-Synchronized Visible and Thermal Face Dataset”. In: *WACV* (2021).
- [26] R. Ranjan, S. Sankaranarayanan, C. D. Castillo, and R. Chellappa. “An All-In-One Convolutional Neural Network for Face Analysis”. In: *FG*. IEEE Computer Society, 2017.
- [27] S. Ren, K. He, RB. Girshick, and J. Sun. “Faster R-CNN: Towards Real-Time Object Detection with Region Proposal Networks”. In: *Advances in Neural Information Processing Systems*. 2015, pp. 91–99.
- [28] S. Umeyama. “Least-squares Estimation of Transformation Parameters Between Two Point Patterns”. In: *IEEE Transactions on Pattern Analysis & Machine Intelligence* 13.04 (1991), pp. 376–380.
- [29] S. Wang, Z. Liu, S. Lv, Y. Lv, G. Wu, P. Peng, F. Chen, and X. Wang. “A Natural Visible and Infrared Facial Expression Database for Expression Recognition and Emotion Inference”. In: *IEEE Trans. Multim.* 12.7 (2010), pp. 682–691.
- [30] Y. Yin, X. Jiang, JP. Robinson, and Y. Fu. “Dual-Attention GAN for Large-Pose Face Frontalization”. In: *15th IEEE International Conference on Automatic Face and Gesture Recognition*. IEEE, 2020, pp. 249–256.
- [31] H. Zhang, VM. Patel, BS. Riggan, and S. Hu. “Generative adversarial network-based synthesis of visible faces from polarimetric thermal faces”. In: *IEEE International Joint Conference on Biometrics, IJCB*. IEEE, 2017, pp. 100–107.
- [32] H. Zhang, BS. Riggan, S. Hu, NJ. Short, and VM. Patel. “Synthesis of High-Quality Visible Faces from Polarimetric Thermal Faces using Generative Adversarial Networks”. In: *Int. J. Comput. Vis.* 127.6-7 (2019), pp. 845–862.
- [33] J. Zhao, Y. Cheng, Y. Xu, L. Xiong, J. Li, F. Zhao, J. Karlekar, S. Pranata, S. Shen, J. Xing, S. Yan, and J. Feng. “Towards Pose Invariant Face Recognition in the Wild”. In: *CVPR*. IEEE Computer Society, 2018, pp. 2207–2216.
- [34] JY. Zhu, T. Park, P. Isola, and AA. Efros. “Unpaired Image-to-Image Translation Using Cycle-Consistent Adversarial Networks”. In: *IEEE International Conference on Computer Vision, ICCV*. IEEE Computer Society, 2017, pp. 2242–2251.
- [35] JY. Zhu, R. Zhang, D. Pathak, T. Darrell, AA. Efros, O. Wang, and E. Shechtman. “Toward Multimodal Image-to-Image Translation”. In: *Advances in Neural Information Processing Systems*. 2017, pp. 465–476.

TABLE VII
CUT-ATC COHORT ANALYSIS ON ARL-VTF DATASET

Gallery	Query	AUC \uparrow	EER \downarrow	TAR@1% \uparrow	TAR@5% \uparrow
0010	00 Baseline	99.5	2.8	91.0	97.9
	10 Baseline	99.7	2.3	94.3	100.0
	11 Baseline	97.1	9.6	59.7	81.7
	00 Expression	99.0	5.2	84.2	94.8
	10 Expression	99.5	3.6	88.0	97.8
	00 Pose	94.1	12.1	63.0	80.9
	10 Pose	95.6	11.0	67.9	82.7
0011	00 Baseline	99.6	2.9	91.4	97.9
	10 Baseline	99.4	3.4	83.7	97.7
	11 Baseline	98.2	7.4	66.3	86.7
	00 Expression	99.0	5.2	84.4	94.8
	10 Expression	98.7	6.2	83.0	93.3
	00 Pose	94.2	12.0	63.2	81.0
	10 Pose	94.2	13.1	61.2	79.5
Average		97.7	6.9	77.2	90.5

TABLE VIII
CUT-ATC COHORT ANALYSIS ON TUFTS DATASET

Gallery	Query	AUC \uparrow	EER \downarrow	TAR@1% \uparrow	TAR@5% \uparrow
Frontal	Frontal	88.2	20.6	31.0	52.3
	Profile	87.6	21.1	23.9	51.7
Profile	Frontal	85.4	23.4	21.4	42.5
	Profile	88.2	20.0	28.4	55.8
Average		87.4	21.3	26.2	50.6

TABLE IX
CUT-ATC COHORT ANALYSIS ON MILAB-VTF(B) DATASET

Gallery	Query	AUC \uparrow	EER \downarrow	TAR@1% \uparrow	TAR@5% \uparrow
Indoor Frontal	Indoor Frontal	76.3	30.6	17.1	34.1
	Indoor Profile	68.3	36.8	9.6	22.4
	Outdoor Frontal	72.8	33.2	12.7	29.0
	Outdoor Profile	64.7	40.1	8.3	20.4
Indoor Profile	Indoor Frontal	68.1	37	9.9	23.3
	Indoor Profile	66.9	37.2	4.3	17.8
	Outdoor Frontal	64.7	39.5	5.8	17.4
	Outdoor Profile	63.4	40.7	5.5	17.3
Outdoor Frontal	Indoor Frontal	74.4	32.2	12.4	29.1
	Indoor Profile	67.9	37.4	7.4	20.4
	Outdoor Frontal	75.5	31.1	12.7	31.3
	Outdoor Profile	65.8	38.9	4.8	18.2
Outdoor Profile	Indoor Frontal	68.8	36.4	6.8	20.6
	Indoor Profile	68.8	36.2	4.9	20.3
	Outdoor Frontal	69.3	35.8	4.0	19.4
	Outdoor Profile	65.8	38.4	1.7	15.4
Average		68.8	36.3	8.0	22.3